From Active Contours to Active Surfaces

Akshaya Mishra
akshaya.mishra.kumar@gmail.com
Tornado Medical Systems

Paul W. Fieguth
pfieguth@uwaterloo.ca
University of Waterloo

David A. Clausi
dclausi@enmail.uwaterloo.ca, University of Waterloo

Abstract

Identifying the surfaces of three-dimensional static objects or of two-dimensional objects over time are key to a variety of applications throughout computer vision. Active surface techniques have been widely applied to such tasks, such that a deformable spline surface evolves by the influence of internal and external (typically opposing) energies until the model converges to the desired surface. Present deformable model surface extraction techniques are computationally expensive and are not able to reliably identify surfaces in the presence of noise, high curvature, or clutter.

This paper proposes a novel active surface technique, decoupled active surfaces, with the specific objectives of robustness and computational efficiency. Motivated by recent results in two-dimensional object segmentation, the internal and external energies are treated separately, which leads to much faster convergence. A truncated maximum likelihood estimator is applied to generate a surface consistent with the measurements (external energy), and a Bayesian linear least squares estimator is asserted to enforce the prior (internal energy).

To maintain tractability for typical three-dimensional problems, the density of vertices is dynamically resampled based on curvature, a novel quasi-random search is used as a substitute for the ML estimator, and sparse conjugate-gradient is used to execute the Bayesian estimator. The performance of the proposed method is presented using two natural and two synthetic image volumes.

1. Introduction

Deformable model based segmentation has been widely used throughout computer vision: in medical image analysis [1, 2], surface reconstruction [3, 4, 5], feature extraction [6], visual tracking [7], and motion estimation [8]. As illustrated in Fig. 1, surface extraction techniques are essential to segment and quantify important structures of volumetric images for successful recognition or diagnosis.

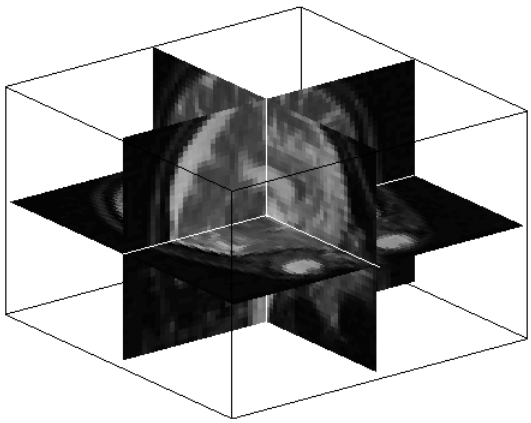

Figure 1. MRI of a human brain: producing a 3D segmentation of such data has countless applications in diagnosis and treatment.

Active surfaces, the three-dimensional generalization of two-dimensional active contours, are a popular approach for such surface extraction. The basic idea of active surfaces is to evolve a deformable model [6, 9, 10, 11, 12, 13] under the influences of internal (prior) and external (measurement) energies to capture the surface of a 3D object. Typically, the internal energy maintains surface smoothness via some sort of elastic (thin-plate) constraint, whereas the external energy pulls the deformable model towards the desired object boundary, usually defined using an image gradient. Many approaches based on the original active surface concept have been proposed, broadly falling into two categories: parametric [10, 14, 11] and non-parametric [15, 16].

All of these active surface methods are direct extensions of their 2D active contour counterparts to the 3D context. In the parametric case, 3D surfaces are explicitly represented [10, 11] using a regular 2D parametric grid, however the grid-to-surface mapping is not unique and is unevenly spaced, such that parametric surface approaches are not able to capture high-curvature surfaces in the presence of noise

without parameter tuning. In contrast, non-parametric active surfaces [17, 15] are robust to initialization and are capable of finding multiple high-curvature surfaces, however these methods are extremely slow and are intolerant of breaks or gaps in the measured surface.

An example illustrating the tradeoff between a parametric and non-parametric active surface models is shown in Fig. 2. The non-parametric active surface model identifies eight separate surfaces (Fig. 2(b)) of a single broken cube, however, a parametric active surface model finds a single continuous boundary around the broken cube.

Normalized graph cut [18] or spectral clustering is another popular segmentation method that is widely used in computer vision literature. However, the gigantic storage burden requirement makes the method impractical for large 3D object segmentation.

Many of the above problems — lack of robust convergence in the presence of clutter and high computational and storage complexity — are also present in 2D active contours. To address these problems in 2D, Mishra et al. [12] proposed a decoupled active contour (DAC) which successfully identifies the boundary of a single object in the presence of noise and background clutter. Motivated by DAC's robustness, this paper describes the development of a parallel approach, a decoupled active surface (DAS), for identifying the surface of a volumetric 3D object. The novel DAS is computationally efficient, shows good convergence robustness, and is not based on a mapped grid, thus allowing the segmentation of more complex geometries.

The rest of the paper is organized as follows. Section 2 is a brief discussion on the theory of parametric active surfaces, followed by identifying the limitations of traditional approaches. The theory and implementation of DAS are provided in Section 3, with experimental results and validation provided in Section 4.

2. Active Surface Theory

An active surface is a generalized energy-minimizing 3D spline [9, 10, 11], represented using a regular grid $v(s,r) = [x(s,r), y(s,r), z(s,r)]$, whose total energy is expressed as

$$E = \int_0^1 \int_0^1 \left(E_{\text{int}}(v(s,r)) + \beta E_{ext}(v(s,r))\right) dsdr. \quad (1)$$

where $E_{\text{int}}(v(s,r))$ and $E_{ext}(v(s,r))$ are the internal and external energies, respectively, of the active surface. The internal energy asserts the prior or inherent constraints on the surface, typically penalizing slope and/or curvature terms:

$$E_{\text{int}}(v(s,r)) = \alpha_1 \left(\frac{dv}{ds}\right)^2 + \alpha_2 \left(\frac{dv}{dr}\right)^2 + \alpha_3 2 \left(\frac{d^2v}{dsdr}\right)^2 + \alpha_4 \left(\frac{d^2v}{ds^2}\right)^2 + \alpha_5 \left(\frac{d^2v}{dr^2}\right)^2. \quad (2)$$

The weights α_i and β controls the influence of the internal and external energies. The external energy creates an attractive force towards the desired boundary, normally a region of high gradient:

$$E_{ext}(v(s,r)) = -\left(\nabla G_\sigma * I_3\right)^2 (v(s,r)), \quad (3)$$

Here ∇ is a derivative operator, G_σ is a Gaussian kernel of bandwidth σ, and I_3 is a series of images representing a volume. A desired surface is usually obtained by minimizing the total energy E of the active surface v.

To illustrate the typical problems of the traditional active surface, the convergence of (1) is demonstrated in Fig. 3(a) using a synthetic volumetric cube (red) with a spherical initial solution (black). For traditional representation schemes which map a 2D grid to the 3D surface, boundary condition enforcement is a complicated task, as shown in Fig. 3(b), (c) and (d). Using free boundary and free pole conditions in (1), a broken surface is generated (Fig. 3(b)), similarly a free pole condition generates holes at both poles of the converged surface (Fig. 3(c)), whereas constrained boundary and poles lead to a biased internal force which creates a non-uniform vertex motion, such that the vertices near the poles have a lower velocity compared to other vertices (Fig. 3(d)).

In summary, the following three problems are prevalent with the conventional active surface based representation scheme and solution technique:

- The conventional 3D surface representation scheme $v(s,r)$ is not able to handle complex geometries; even in cases where the geometry can in principle be represented, the 2D-3D mapping creates a biased internal force, as seen in Fig. 3(d).
- The conventional active surface is a direct extension of 2D active contour to 3D and uses iterative gradient descent to solve (1). Such an iterative solver is very slow and sensitive to local minima.
- There exists a delicate relationship between the weights (parameters) in (1).

Most of the present parametric active surface methods, such as gradient vector flow (GVFS) [11] and vector field convolution (VFC) [10], have attempted to solve some of these problems (sensitivity to initial solution and inability to converge towards concave regions) by increasing the capture range of the traditional active surface by diffusing the traditional gradient-based external force. However, these modifications are not able to overcome the problems of local minima and convergence speed.

3. From Decoupled Active Contours to Decoupled Active Surfaces

The decoupled active contour proposed by Mishra et al. (DAC) [12] has as its principle novelty a decoupling (Fig. 4)

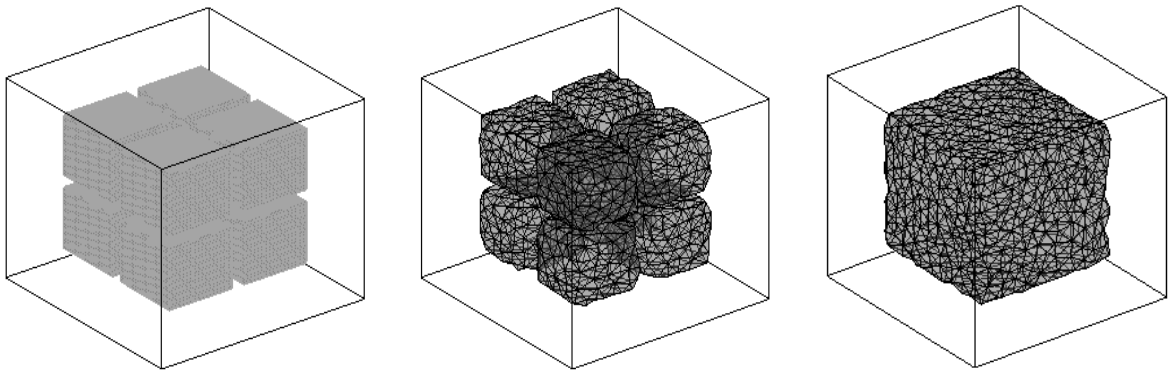

(a) Volumetric image (b) Non-parametric surface (c)Parametric surface

Figure 2. Example of the suitability of parametric active surfaces over non-parametric active surfaces. (a) An image of a broken cube. (b) Non-parametric active surface identifies eight separate surfaces. (c) Parametric active surface finds a single connected surface of the broken cube.

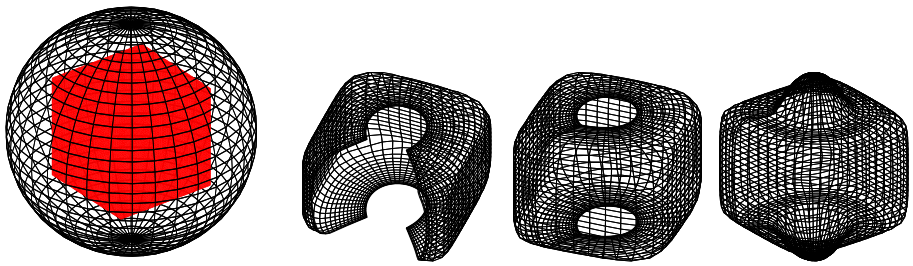

(a) Initial boundary (b) Free pole and boundary (c) Constrained boundary and free pole (d)Constrained boundary and pole

Figure 3. Three examples (b, c and d) illustrating the convergence of traditional, parameterized active-surface schemes. We start with an initial, parameterized spherical surface (a), seeking to converge to the red synthetic cube. The partially-converged active surfaces after 500 iterations are shown in panels (b), (c) and (d). Parametric models have difficulties with boundaries (b) and singularities at poles (c,d).

of the internal and external energy terms, on the premise that together the energies are difficult to optimize, whereas individually the solution is much more straightforward, so a conditional coordinate-descent approach leads to exceptionally fast convergence.

The method optimizes the external energy by applying a dynamic programming (Viterbi search) method, and the internal (prior) energy by asserting a linear Bayesian estimator. High-curvature boundaries are preserved by using a non-stationary prior, obtained by non-uniform point spacing along the contour, where an importance sampling step is used, based on curvature, to generate the points.

We find the basic premise (internal-external energy decoupling, curvature-based re-sampling) highly motivating, however there are significant problems with the straightforward extension of the method to surfaces in three dimensions. The Viterbi search is not practical on a 3D trellis (shown in Fig. 5) since causality fails, the definition of curvature and mesh re-sampling is far more elusive on a set of vertices in 3D relative to points along a 2D curve, finally very large numbers of active surface vertices are needed to represent the surface, leading to unacceptably large computational and storage requirements for a Bayesian estimation step. The purpose of this paper is address these three limitations, to obtain a fast, robust segmentation method for 3D objects. Each of the novel developments is described in the subsections below.

3.1. Iterative Quasi Random Search (IQRS) for Surface Identification

The ML estimator / Viterbi method of [12] are too slow for 3D:
We propose an iterative quasi-random search (IQRS) to find an optimal surface within a specified search space. The search space is created using a discrete 3D trellis and a quasi-random number generator [19, 20], and the problem of finding the best surface is modeled as a hidden Markov model (HHM).

Fig. 5 shows the 3D trellis, such that the active surface $\mathbf{v}$ is represented using a set of q vertices

$$v_j = v_{z_j|z_j=0} = (x_{j,0}, y_{j,0}, z_{j,0}), j \in [1, q] \qquad (4)$$

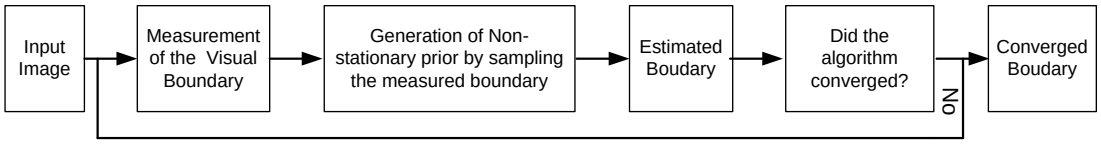

Figure 4. Common flow diagram for DAC and DAS

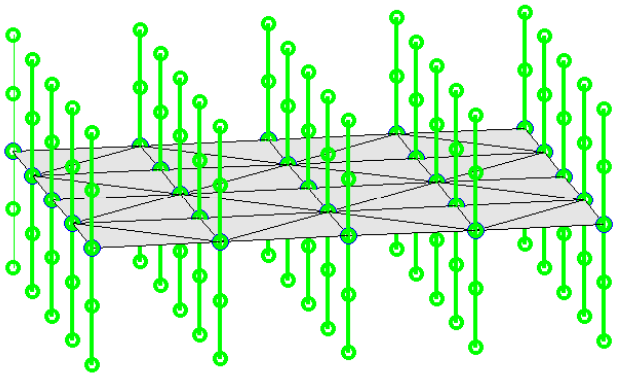

Figure 5. Example 3D trellis used in iterative quasi random search. The initial grey surface $v_j = v_{z_j|z_j=0}, j \in [1,q]$ is triangulated using conforming triangles (black). Each search normal (green) contains $2 \times u + 1$ nodes. In this illustration, $q = 25$ and $u = 2$.

and f triangular faces. Given a face f_k, the three vertices corresponding to face f_k are defined as

$$Z\left(f_k\right) = [v_{a_{f_k}}, v_{b_{f_k}}, v_{c_{f_k}}]. \tag{5}$$

Similarly, the neighboring vertices of a vertex v_i are given by $v_{\Omega_{z_j=i}}$. For efficiency, both Z and Ω are stored as look-up tables.

At each of the q vertices shown in Fig. 5, a set of $2*u+1$ points are defined lying (along a line) evenly spaced normal to the surface. The possible set of solutions over which an optimization algorithm is carried out is presented using a graph, representing the search space. The hypothesis of a node i belonging to a surface $\mathbf{v}$ is computed from the external energy E_{ext} and modeled as $p(E_{ext}|v_{z_j=i})$, the observation probability. To avoid noise, a transition probability $p(v_{z_j=i}, v_{\Omega_{z_j=i}})$ for a node is computed using the Euclidian distance of the current node $v_{z_j=i}$ from its first-order neighboring nodes $v_{\Omega_{z_j=i}}$. The pseudo-code for IQRS algorithm is provided in Algorithm 1.

The optimal boundary $\mathbf{v}_k^m$ using IQRS is assigned as the measured boundary at iteration k. A non-stationary prior is essential in the update step to capture high curvature boundaries. The generation of the non-stationary prior using curvature based mesh re-sampling and update step follows.

3.2. Curvature Based Mesh Re-sampling

The definition of curvature is much more subtle on an implicit 3D vertex set than on a 2D curve:
High curvature regions (corners, edges) of a surface can captured by relaxing the prior. This has been accomplished via an importance sampling step in 2D, placing a greater density of samples near regions of high curvature [12].

The curvature κ of a parametric 2D curve $v(s) = [x(s), y(s)]$ is defined as the rate of change of tangent angle with respect the arclength s. However for a 3D surface the curvature at a particular point varies as the plane through the normal at that point changes, therefore there is no unique definition of surface curvature. 3D curvature is usually defined using principal and Gaussian curvatures, however for our purposes an exact definition of curvature is not needed, rather what is needed is some measure of triangulation error, such that additional triangles are placed near edges and corners. By using least squares to fit a plane to the first-order neighboring vertices v_{Ω_i}, the pseudo curvature κ_i can be represented as the perpendicular distance from surface node i to the plane.

Having computed κ at all vertices, Algorithm 2 produces the resampled set of vertices, such that faces with curvature exceeding a threshold κ_{th} are considered for subsampling, and then along the longest edge of that face. Reducing the number of vertices is a far more difficult operation, therefore the method is initialized with a deliberately small num-

Algorithm 1 $[\mathbf{v}_k^m]$ = Function IQRS($\mathbf{v}_{k-1}^e$, ϵ)

Obtain the states $\ell_j, j \in [1,q]$ corresponding to high gradient locations as:
$\ell_j = \underset{i=[-u:u]}{\arg\max} \left(p\left(E_{ext}|v_{\mathrm{z_j|z_j=i}}\right)\right), j = \{1, 2 \cdots q\}$
Assign $\mathbf{v}_k^m = \mathbf{v}_{k-1}^e$ (Previous estimated boundary)
repeat
  Let $r = \{\cdots\}_q$ be a sequence of q quasi random numbers generated using a quasi random number generator [19, 20].
  Assign $\mathbf{vp}_k^m = \mathbf{v}_k^m$ and $\ell_j^p = \ell_j, j \in [1,q]$
  for $j \in r$ **do**
    Update the values of ℓ_j as:
    $\ell_j = \underset{i=[-u:u]}{\arg\max} \left(p\left(E_{ext}|v_{\mathrm{z_j|z_j=i}}\right) p\left(v_{\mathrm{z_j|z\_j=i}}, v_{\Omega_{\mathrm{z_j=}\ell_j^p}}\right)\right)$
  end for
  $\mathbf{v}_k^m = v_{\mathrm{z_j|z\_j=}\ell_j}$
until $\|\mathbf{v}_k^m - \mathbf{vp}_k^m\| \leq \epsilon$

Algorithm 2 $[\mathbf{v}_{out}]$ = Function 3DResample($\mathbf{v}_{in}$, κ_{th}, l_{th})

$\mathbf{v}_{out} = \mathbf{v}_{in}$
while $j \leq q$ **do**
  Compute the pseudo curvature κ_j
  if $\kappa_j > \kappa_{th}$ **then**
    Get all the edges $e(j)$ that are connected to the vertex j
    Get the longest edge length l_l and the index i corresponding to l_l from the length $l(e_i(j))$ of all edges.
    if $l_l > l_{th}$ **then**
      Bisect the edge $e_i(j)$ by inserting a new node and update $\mathbf{v}_{out}$
      Update the $\mathbf{v}_{out}$
    end if
  end if
  $j = j + 1$.
end while

ber of vertices, with further vertices added as needed, but never removed.

3.3. Statistical Estimation

The 3D problem is far too large to undertake a simple Bayesian estimator:
In principle, the surface nodes could be identified purely using the Viterbi-like IQRS method of Algorithm 1, however IQRS does not admit the assertion of complex shape priors or noise statistics. Since both the prior model and measurement model are essential for the robust convergence of a contour or surface in the presence of noise, therefore some sort of Bayesian step is needed. The exact (e) and measured (m) nodes of a surface can be expressed as

$$x_k^m = x_k^e + \eta, \;\; y_k^m = y_k^e + \eta, \;\; z_k^m = z_k^e + \eta \qquad (6)$$

where $\eta \sim N(0, R_k)$, $x_k^e \sim N\left(\mu_{x_k^e}, P_k\right)$, $y_k^e \sim N\left(\mu_{y_k^e}, P_k\right)$, and $z_k^e \sim N\left(\mu_{z_k^e}, P_k\right)$. The Bayesian linear least-squares estimator can be formulated as [21]

$$\mathbf{x}_k^e = \left(R_k^{-1} + P_k^{-1}\right)^{-1} R_k^{-1} \mathbf{x}_k^m, \qquad (7)$$

where similar expressions hold for y_k and z_k. The measurement uncertainty matrix R_k is a diagonal matrix where each diagonal component (the noise variance) is computed empirically from a local window. Following the conventional active surface formulation, DAS asserts a second-order penalty as prior in $Q_k = P_k^{-1}$. For a reasonably sized mesh of $q = 5000$ vertices, the dimensionality of the constraint matrix Q_t is 5000×5000, clearly making the direct solution of (7) impractical.

However Q_k and R_k are highly sparse, therefore the system matrix $\left(R_k^{-1} + Q_k\right)$ is also sparse, allowing (7) to be solved very efficiently using implicit, iterative methods. We propose to use conjugate gradient, solving (7) as a linear system

$$\underbrace{\left(R_k^{-1} + Q_k\right)}_{A} \hat{\mathbf{x}}_k = \underbrace{R_k^{-1} \mathbf{x}_k^m}_{b} \qquad (8)$$

Since conjugate gradient requires only the matrix-vector product $A\mathbf{x}$, and since the entries in A represent a fixed constraint, and those in R computed from the image, therefore neither Q nor R require storing explicitly, even in sparse form, and an implicit functional representation is used to dynamically compute $A\mathbf{x}$.

4. Testing and Discussions

The capabilities of DAC to segment 2D objects in the presence of noise and background clutter have been demonstrated [12]. DAS generalizes the DAC concepts to 3D and validates its claims using three natural and synthetic 3D volumetric images and two 2D moving image sequence. The four test cases involve a wide range of characteristics including high curvature and noise. The proposed DAS is compared to the vector field convolution (VFC) [10] active surface method.

We downloaded the code for VFC from [22] and utilized the code for testing. All experiments are performed on a P4 Intel 2.4Ghz processor, 1Gb RAM using MATLAB. The parameters for VFC are adopted from [10]. In the proposed approach the parameters: $\kappa_{th} = 1$, $l_{th} = 8$, $\alpha_1 = 0.1$, $\alpha_2 = 0.1$, $\alpha_4 = 0.05$, $\alpha_5 = 0.05$ and $\alpha_3 = 0$ are used for all test cases. Both approaches are initialized with a spherical initial surface . DAS's ability to identify the surface of 3D volumetric images is presented in Figs. 6 and 7.

Fig. 6 compares the performance of DAS (middle) and VFC (right). VFC was unable to identify either synthetic surface (A and B). The unbiased internal force created due to the conventional representation scheme used in VFC smoothed the high curvature portion of the U-shaped object. In contrast, the DAS successfully identified the high curvature surface regions of both objects A and B, using separated measurement and prior steps, and also by enforcing a lower force in high curvature regions. The high-curvature tolerance of DAS is illustrated most clearly in the sharpness of the top and bottom surface edges in image (B).

The convergence time of DAS compared to VFC is presented in Table 1. The convergence time of DAS is clearly significantly lower than that of VFC.

VFC requires a large number of nodes in order to segment natural volumetric images. The current MATLAB implementation of VFC is not able to handle more than $q = 5000$ mesh nodes, therefore we are unable to present VFC results for natural volumetric images. The ability of DAS to identify the outer surface of a human head in a volumetric MR image, and the trajectory of a walking man in

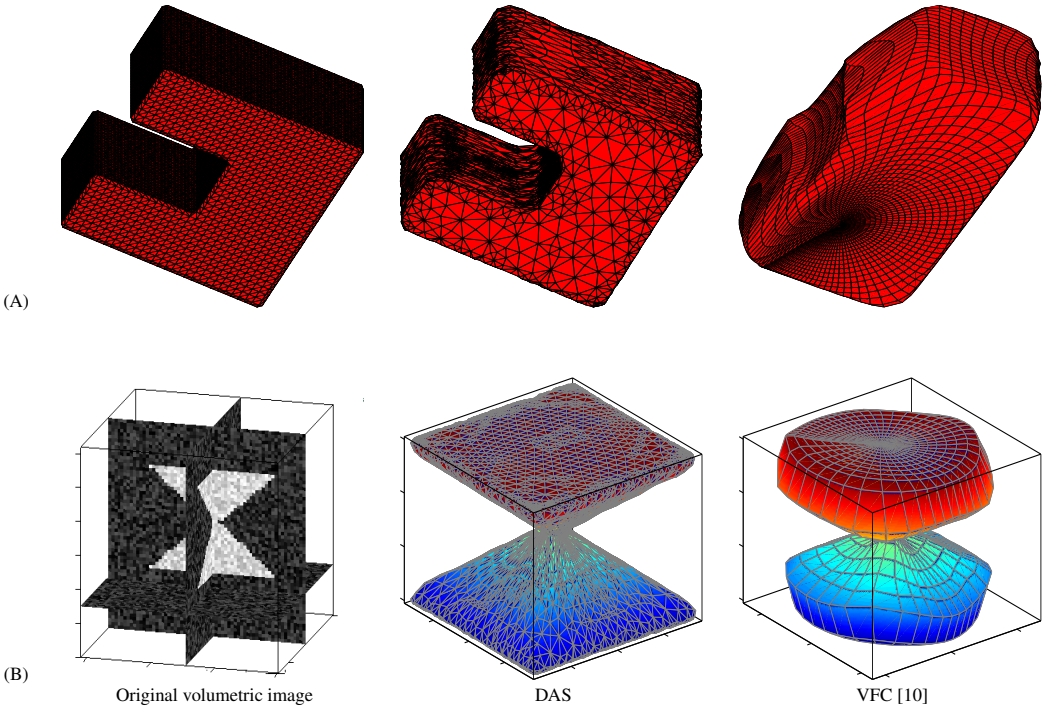

Figure 6. Boundary identification accuracy of DAS and VFC using two surfaces: a U-shape (A), top, and a noisy twin inverted conical volume (B), bottom. DAS (center column) segments both of these objects successfully, note particularly the sharpness of the cone edges, however VFC (right column) is ineffective for both objects.

Table 1. Comparison table showing execution time in seconds for the surfaces in Fig. 6, comparing DAS and VFC [10]. DAS is more than an order of magnitude faster than VFC.

	A (u-shape)	B (inverted twin cone)	C (MRI Brain)	D (walk sequence)	E (walk sequence)
(DAS)	**323**	**179**	297	512	539
(VFC)	12853	11232	-	-	-

a spatio-temporal sequence [23] are demonstrated in Figs. 7 and 8, respectively. In both cases, DAS successfully identified high curvature regions (e.g., the ears, nose and eyes in the MR image) the human walking trajectory.

5. Conclusions

This paper proposed a novel decoupled active surface (DAS) for identifying the surface of static 3D objects and moving 2D objects in volumetric imagery. DAS is a significant three-dimensional generalizatoin of the decoupled active contour (DAC) used for identifying boundaries in 2D imagery. DAS has achieved dramatic improvements in computational requirements and segmentation accuracy compared VFC, a current parametric active surface method.

The computational efficiency of the DAS method is due to the use of decoupled prior-measurement terms, and due to the use of efficient approaches for the measurement and prior assertions. The high curvature tolerance of the method is due to the novel resampling method, implicitly making the prior non-stationary, weakening it in areas of high curvature and allowing the surface to accommodate sharp folds.

References

[1] Davatzikos, C., Prince, J.: An active contour model for mapping the cortex. IEEE Transactions on Medical Imaging **14** (1995) 65–80

[2] Tsechpenakis, G., Wang, J., Mayer, B., Metaxas, D.: Coupling CRFs and deformable models for 3d medical image segmentation. In: IEEE Computer Scociety Work Shop on Mathmatical Methods in Biomedical Image Analysis. (2007) 1–8

[3] Knopf, G., Sangole, A.: Freeform surface reconstruction from scattered points using a deformable spherical map. International Journal of Image and Graphics **6** (2006) 341–356

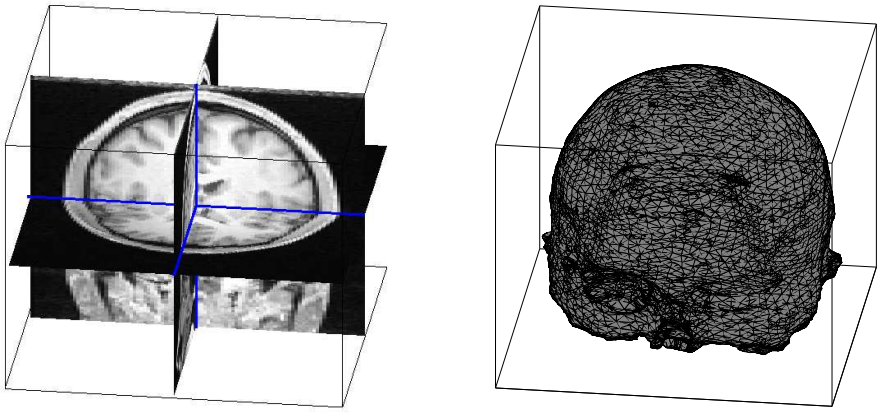

(a) Volumetric brain MRI (b) DAS

Figure 7. Image C: a human MRI scan. DAS successfully identified the outer surface of the MRI of the brain, whereas VFC (not shown) failed to converge meaningfully.

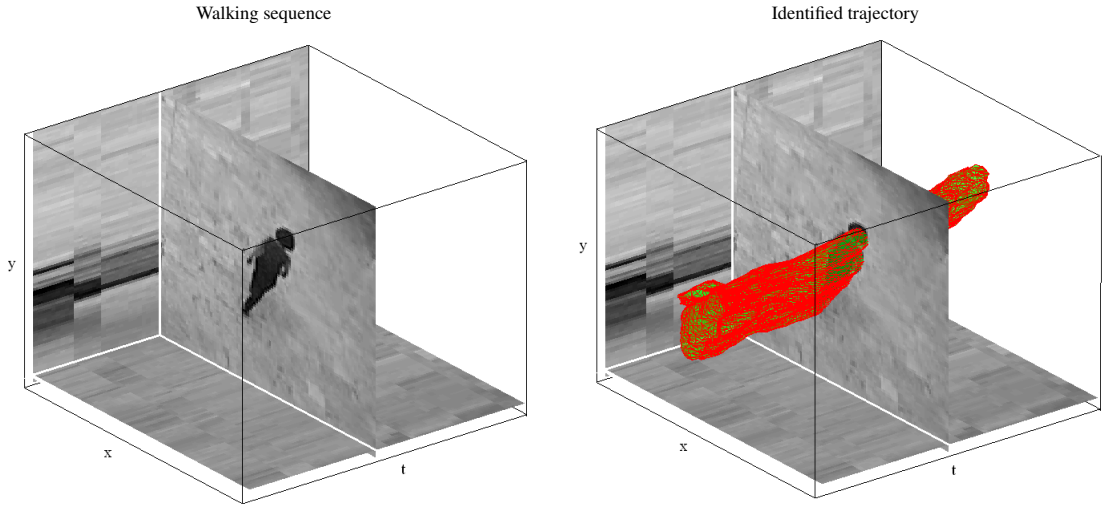

Figure 8. Image D: (a) Trajectory of a moving 2D object (collected from the PETS 2007 data sets [23]), namely a man walking. (b) DAS successfully identified the desired surface traced by the walking man. The trajectory is shown in red and for clarity three slices in $x - y$, $y - t$, and $x - t$ planes are presented in the left panel. The dark object is the walking man.

[4] Pons, J., Boissonnat, J.: Delaunay deformable models: Topology-adaptive meshes based on the restricted delaunay triangulation. In: IEEE Computer Society Conference on Computer Vision and Pattern Recognition. (2007) 1–8

[5] Brostow, G.J., Shotton, J., Fauqueur, J., Cipolla, R.: Segmentation and recognition using structure from motion point clouds. In: European Conference on Computer Vision, Berlin, Heidelberg, Springer-Verlag (2008) 44–57

[6] Krueger, M., Delmas, P., Gimel'Farb, G.: Active contour based segmentation of 3d surfaces. In: European Conference on Computer Vision, Berlin, Heidelberg, Springer-Verlag (2008) 350–363

[7] Varanasi, K., Zaharescu, A., Boyer, E., Horaud, R.: Temporal surface tracking using mesh evolution. In: European Conference on Computer Vision. (2008) II: 30–43

[8] Zhang, J., Gao, J., Liu, W.: Image sequence segmentation using 3d structure tensor and curve evolution. IEEE Transactions on Circuits and Systems for Video Technology **11** (2001) 626–6411

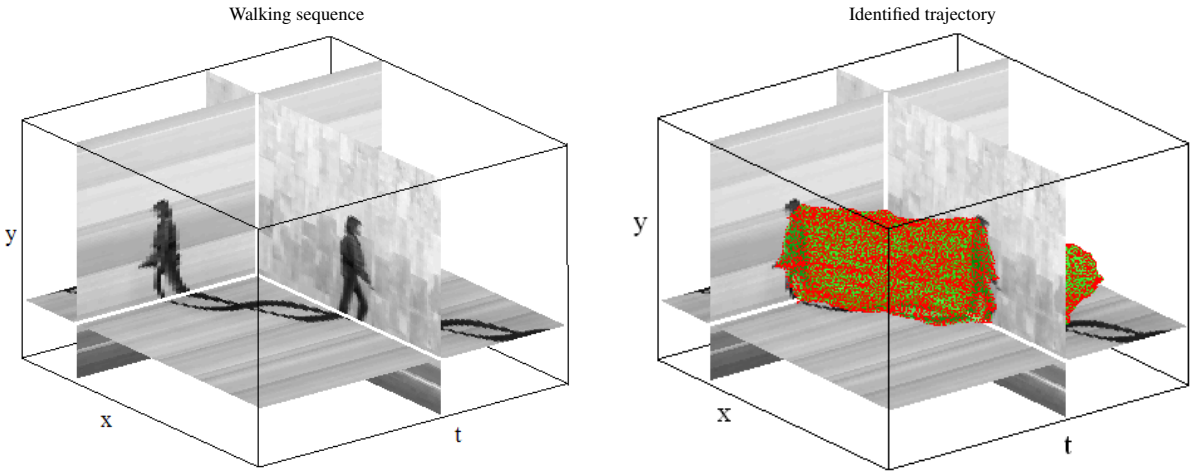

Figure 9. Image E [24]: Image sequence of a moving 2D object, left. At first glance, it would appear that there are two people, however they are the same person, once sliced in space (fixed in t) and the other sliced in time (fixed in x). The tunnel, right, is shown in green (face color) and red (edge color).

[9] Kass, M., Witkin, A., Terzopoulos, D.: Snakes: Active contour models. International Journal of Computer Vision **1** (1988) 321–331

[10] Li, B., Acton, T.: Active contour external force using vector field convolution for image segmentation. IEEE Transactions on Image Processing **16** (2007) 2096–2106

[11] Xu, C., Prince, J.: Snakes, shapes, and gradient vector flow. IEEE Transactions on Image Processing **7** (1998) 359–369

[12] Mishra, A., Fieguth, P., Clausi, D.: Decoupled active contour (DAC) for boundary detection, preprint,. IEEE Transactions on Pattern Analysis and Machine Intelligence **99** (2010)

[13] Mille, J., Boné, R., Cohen, L.D.: Region-based 2d deformable generalized cylinder for narrow structures segmentation. In: European Conference on Computer Vision, Berlin, Heidelberg, Springer-Verlag (2008) 392–404

[14] Slabaugh, G., Unal, G.: Active polyhedron: Surface evolution theory applied to deformable meshes. In: IEEE Computer Society Conference on Computer Vision and Pattern Recognition. (2005) II: 84–91

[15] Chan, T., Vese, L.: Active contours without edges. IEEE Transactions on Image Processing **10** (2001) 266–277

[16] Debreuve, E., Barlaud, M., Aubert, G., Laurette, I., Darcourt, J.: Space-time segmentation using level set active contours applied to myocardial gated spect. IEEE Transactions on Medical Imaging **20** (2001) 643–659

[17] Caselles, V., Kimmel, R., Sapiro, G.: Geodesic active contours. International Journal of Computer Vision **22** (1997) 61–97

[18] Shi, J., Malik, J.: Normalized cuts and image segmentation. IEEE Transactions on Pattern Analysis and Machine Intelligence **24** (2000) 888–905

[19] Sobol, I.: Uniformly distributed sequences with an additional uniform property. USSR Computational Mathematics and Mathematical Physics **16** (1976) 236–242

[20] Mishra, A., Wong, A., Clausi, D.A., Fieguth, P.: Quasi-random nonlinear scale space. Pattern Recognition Letters **31** (2010) 1850 – 1859 Meta-heuristic Intelligence Based Image Processing.

[21] Fieguth, P.: Statistical Image Processing and Multidimensional Modeling. Springer Verlag, 454pp (2010)

[22] Li, B., Acton, A.: Verginia image and video analysis, vector field convolution (2009) http://viva.ee.virginia.edu/researchvfc/.

[23] PETS: Tenth ieee international workshop on performance evaluation of tracking and surveillance (2007) http://pets2007.net/.

[24] Gorelick, L., Blank, M., Shechtman, E., Irani, M., Basri, R.: Actions as space-time shapes. IEEE Transactions on Pattern Analysis and Machine Intelligence **29** (2007) 2247–2253